Programmable constitutive mode-coupling in tubular origami metamaterials

Article · June 2025

DOI: 10.1038/s44455-025-00004-7

3 authors:

Aditi Sharma
University of Southampton
13 PUBLICATIONS **4** CITATIONS
SEE PROFILE

Susmita Naskar
University of Southampton
129 PUBLICATIONS **1,428** CITATIONS
SEE PROFILE

Tanmoy Mukhopadhyay
University of Southampton
295 PUBLICATIONS **6,321** CITATIONS
SEE PROFILE

Programmable constitutive mode-coupling in tubular origami metamaterials

A. Sharma[a], S. Naskar[a], T. Mukhopadhyay[a*]

[a]*School of Engineering, University of Southampton, Southampton, UK*
[*]*Email address: t.mukhopadhyay@soton.ac.uk*

Abstract

Metamaterials and metastructures developed based on tubular origami-inspired structural forms can leverage the convolution of crease architecture and the mechanics of deformation therein to provide unique multi-functional properties. In the existing literature, the intriguing aspect of deformation mode coupling between the axial and twisting modes in different classes of origami tubes has not been explored adequately. Based on computational and experimental investigations, here we present novel exploitable insights on tunable axial-twist coupling behaviour in tubular origami metamaterials, including the aspect of programming Poynting effects as a function of triangulated crease architecture. We focus on exploring whether there can be twisting or axial deformation under the application of either axial or twisting far-field actuation in a compulsory or discretionary way, and the functional relationship to modulate such constitutive coupling through triangulated crease architecturing. The corresponding energy landscapes are investigated, revealing their stability behaviour and the prospect of crease-dependent tailoring of multi-stability.

Keywords: Origami metamaterials; Tubular origami; Poynting effect; Bi-stability programming; Constitutive mode coupling; Triangulated crease architecture

1. Introduction

Mechanical metamaterials [1], driven by the recent progress in manufacturing technologies for complicated topologies [2, 3], have surged in popularity over the last decade due to their innovative approach in incorporating bottom-up lower-length scale architectures with intricate micro- and nano-scale designs to achieve unprecedented mechanical and multi-physical attributes (at a relatively higher length scale) which are not available in naturally-occurring materials [4–9]. The effective mechanical attributes in metamaterials are often driven by the geometry of unit cells along with the intrinsic material properties, leading to the possibility of modulating the effective mechanical behaviour as a function of lower-length scale architectures maintaining invariance of the base intrinsic material. These architected materials are artificially manufactured using conventional materials (referred to as intrinsic materials), often organized in repetitive patterns at scales smaller than the wavelengths they influence for a dynamic system. In the case of evaluating static effective properties, it is ensured that there exists a significant difference in the length scales of unit cell geometry and the higher length scale at which the effective properties are defined, resulting in a converged number of unit cells without boundary effects. In

case of the absence of an adequate number of unit cells such that homogenised properties cannot be evaluated, the term 'metastructure' is defined in the literature (note that even metastructures possess exotic properties attributed to the designed geometric architecture). In general, metamaterials derive their unique capabilities not only from their constituent materials unlike conventional materials (where chemical compositions derive the mechanical properties), but from the deliberate design of their lower-scale architectures as well through precise shaping, sizing, orientation, and arrangement. This leads to the manipulation of static and dynamic properties exceeding the capabilities of traditional materials, offering a wide range of possibilities for various engineering applications [1, 10–16]. Two primary classes of metamaterial architectures are typically conceptualized based on lattice and origami base patterns [1, 17, 18]. The central theme of this paper is origami-inspired metamaterials wherein we will focus on tubular origami architectures due to their inherent advantages such as geometric efficiency and compactness, deployability and reconfigurability, structural integration ability in complex shapes, stiffness and strength modulation, constitutive programming and deformation mode coupling, high specific energy absorption capability, controlled transportation of fluid and gas, multi-stability and programmable dynamic behaviour [19–27].

Unlike lattice-based metamaterials that derive their unique properties from intricate beam, plate or shell-based unit cells [1], origami and kirigami-inspired metamaterials primarily exploit geometric principles and mechanics of folding to create periodic functional architectures [28–30]. Origami, a traditional Japanese paper-folding technique, involves the transformation of two-dimensional sheets of material into intricate three-dimensional architecture through the introduction of predefined creases for folding [31, 32]. In comparison, kirigami is a technique that involves cutting paper along with folding. Metamaterials are formed when such origami or kirigami base patterns are tessellated in one, two or three-dimensional spaces to form a periodic architecture. Over time, for engineering applications of origami and kirigami, there has been a transition from traditional paper to a diverse array of materials such as metals, smart material alloys, polymers, and hydrogels, expanding the possibilities and functionalities of these origami and kirigami-inspired metamaterials. Origami-based tubes (refer to Figure 1) are formed by folding a sheet of material into a tessellated architecture and often rolling it to give a hollow cylindrical shape, which leads to a range of enhanced mechanical and multi-physical features [33–40]. Some of the prominent tubular origami architectures include Miura-ori [41, 42], waterbomb [43–46], Yoshimura [47–52] and Kresling [32, 53–58], among which we will primarily concentrate on triangulated crease patterns such as waterbomb and Kresling architectures in this paper due to their unique constitutive traits concerning deformation mode coupling behaviour.

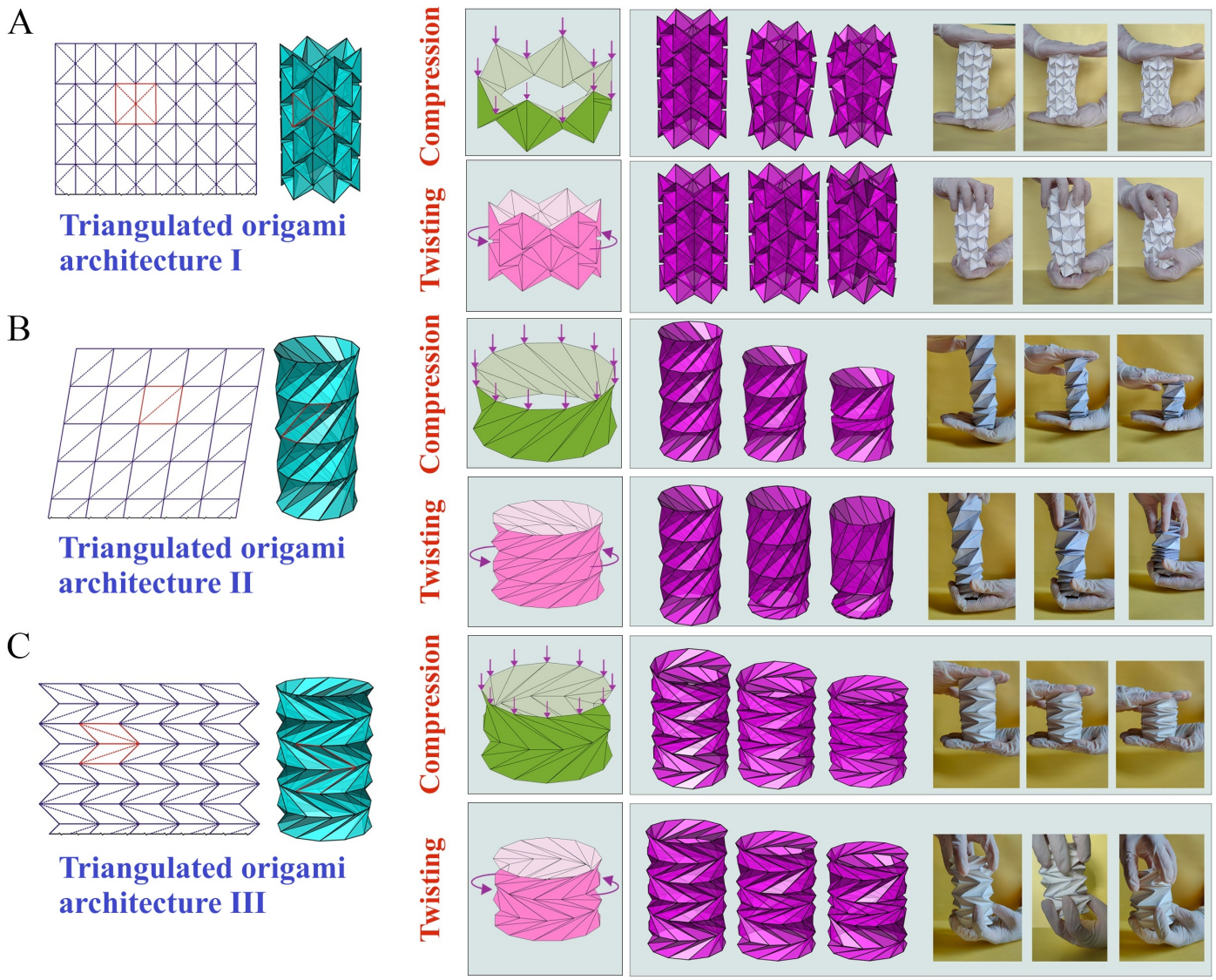

Figure 1: Crease-architecture driven deformation-mode coupling and programmable multi-stability. Crease architecture and the resulting tubular metamaterials showing the deformation behaviour under axial compression and twisting moment based on numerical models and experimental prototypes. **(A)** Triangulated origami architecture I **(B)** Triangulated origami architecture II **(C)** Triangulated origami architecture III.

Waterbomb unit cells, as typically adopted in tubular metamaterials with triangulated crease patterns, comprise a square sheet of material having six creases: four diagonal creases acting as valley creases intersecting at a common vertex and two collinear sides acting as mountain creases (refer to Figure 1(A)). Through repetitive tessellation of the waterbomb unit cell in both longitudinal and circumferential directions, a waterbomb tube is formed, exhibiting rich mechanical characteristics [59] in terms of programming constitutive laws, auxetic behaviour and shape modulation. Additionally, the symmetrical folding of the waterbomb tube makes it a single-degree-of-freedom system [43–46] that requires limited actuation. Interestingly, it may be noted that since each of the waterbomb units is inherently bistable along the radial direction, it leads to a possibility of further programming the mechanical behaviour based on selective stable state distribution. Based on the common theme of this

paper concerning triangulated origami creases, we refer waterbomb tubes as triangulated origami architecture I in the following sections. Waterbomb tubes find critical applications in the construction of origami robots, medical devices [60] and the design of wheels suitable for autonomous navigation [61]. Fonseca et al. proposed an expandable origami wheel, constructed based on the fundamental principles of the waterbomb pattern undergoing transitions between various configurations via thermal actuation enabled by shape memory alloy actuators [62]. Its deployment gives rise to a lot of benefits, including trajectory adjustments through alteration of configuration, obstacle traversal capabilities, and enhanced stability during rolling movements. Li et al. proposed the architecture of a simple soft gripper involving waterbomb origami [63]. This gripper is evaluated by capturing a range of everyday objects as well as a set of test objects with diverse geometries.

One of the most versatile bases in the design of origami tubes with triangulated crease patterns is Kresling which can show a range of programmable mechanical characteristics based on crease architecture and assembly. Based on the common theme of this paper concerning triangulated origami creases, we have referred to the two primary Kresling patterns here as triangulated origami architecture II and III. The triangulated origami architecture II and III tubes are constructed based on the same Kresling unit, with Type II utilizing units of the same handedness and Type III employing an alternating handedness configuration (refer to figure 1(B, C)). In this context, it will be demonstrated later in this manuscript that such configurational changes with even similar triangulated patterns can bring marked differences in the characteristic constitutive behaviour. The triangulated origami architecture II base consists of a parallelogram sheet designated by five creases, with four sides of the parallelogram acting as mountain folds and one vertical diagonal functioning as a valley fold. Through repetitive tessellation of triangulated origami architecture II unit cells in both longitudinal and circumferential directions, a tube is formed [64] (refer to Figure 1(B)). Notably, the triangulated origami architecture II based tube lacks rigid foldability and cannot deviate from its nominal expanded state through crease manipulation. Upon reaching its fully folded state, the upper and lower triangular planes align with each other. A distinguishing characteristic of these tubular metamaterials lies in its multi-stability, which depends upon the tube's height and the length of its diagonal [53–56]. One notable application of the triangulated origami architecture II is in the development of multi-degree-of-freedom origami robots that achieve motion by electro-thermal actuation, resembling a caterpillar [65]. This technology offers several advantages, including its lightweight design, ability to execute steering motions by assembling with other robotic units and cargo transportation.

The triangulated origami architecture III pattern draws inspiration from the geometric structure of

unfolded tree leaves. It is characterized by a tessellation process where triangulated origami architecture III bases are repetitively arranged longitudinally and circumferentially to form a tube. The base here comprises two identical parallelograms positioned adjacent with sharing a common side and it additionally includes two vertical diagonals in opposite alignment converging at a common vertex. Triangulated origami architecture III unit cells comprise nine creases, with all seven sides acting as mountain creases and the two diagonals acting as valley creases (refer to Figure 1(C)). Triangulated origami architecture III based tubes exhibit partial flat folding exclusively at the region of valley creases, while remaining essentially three-dimensional in already bent regions [66–69]. However, it lacks rigid foldability and can exhibit mono-stability and multi-stability depending on the geometric parameters. Among its practical applications, the triangulated origami architecture III based design can find its utility in the development of magnetically actuated biopsy robot [70]. In this application, the proposed structure enables the robot to fold, deploy the needle into the targeted tissue, effectively capture the tissue and provide the retraction force when external magnetic force is removed. The permanent magnet on the top of the robot generates magnetic force and torque in response to external magnetic field, allowing the robot to effectively perform the rolling and sampling motion. Yasuda et al. proposed triangulated origami cylinders for vibration analysis and dynamic characteristics of structures, while Chung et al. demonstrated these cylinders to serve as piezoelectric generators [71, 72]. Further applications based on triangulated origami architecture III include untethered robots propelled by magnetic actuation [73] and memory switch that can be activated by providing harmonic mechanical excitation at its base [74].

A careful review of the literature concerning tubular origami metamaterials [17, 29] reveals that the intriguing aspect of deformation mode coupling between the axial and twisting modes in different classes of origami tubes has not been explored adequately. Such interaction between axial and twisting modes can be instrumental for designing tailored constitutive behaviour in advanced engineering applications with efficient load distribution and conversion of deformation modes in wave propagation and steering, energy harvesting and vibration control applications. Based on computational and experimental investigations, here we endeavour to present novel exploitable insights on the axial-twist coupling behaviour in tubular origami metamaterials including the aspect of programming Poynting and inverse Poynting effects as a function of crease architecture. We will primarily focus on exploring whether there can be twisting or axial deformation under the application of either axial or twisting far-field actuation (refer to figure 1(A, B, C)) in a compulsory or discretionary way, and the functional relationship to modulate such constitutive coupling through crease architecturing. The corresponding energy landscapes will be investigated as an integral part, revealing the stability behaviour and the prospect of crease

architecture-dependent tailoring of multi-stability. Based on a common triangulated pattern inscribed in the same intrinsic material, such constitutive programming in coupling behaviour, Poynting effect, energy landscape and stability behaviour would be demonstrated through targated architecturing of the creases. The unique and tailorable mechanical constitutive behaviour of tubular metamaterials will lead to diverse applications in the field of mechanical, robotics, space, electronic devices and communication, biomedical, and architecture.

2. Results

The current discussion centres around three major tubular metamaterial architectures based on triangulated crease patterns (refer to figure 1(A, B, C)) with a range of different geometric parameters to investigate their deformation mode coupling and stability behaviour. These crease architectures are chosen in the current paper to demonstrate the crease architecture and motion stage-dependent constitutive coupling behaviour. We would demonstrate that such targeted constitutive programming in tubular metamaterial is feasible through appropriate orientation and assembly of the triangular facets in designing the origami bases. To begin the discussion, we first describe the architecture of these three tubular origami metamaterials under consideration. The triangulated origami architecture I (also referred to as waterbomb origami in the literature) base comprises a square sheet having six creases: two creases parallel to the vertical sides of the square represent the mountain crease, and four diagonal creases represent the valley creases. The triangulated origami architecture II (also referred to as Kresling origami in the literature) base comprises a parallelogram sheet with five creases: four sides of the parallelogram represent mountain creases, and one diagonal represents the valley crease. The triangulated origami architecture III (also referred to as Kresling origami in the literature) base comprises two identical parallelograms with mirror configurations connected to a common side. These parallelograms are arranged in series on the vertical axis, with nine creases: seven sides of the parallelogram represent mountain creases, and two diagonals represent valley creases. These unit cells are repeatedly arranged in series along vertical and circumferential directions to obtain a tubular configuration of the metamaterial, as depicted in Figure 1 (sometimes a row in the vertical direction is referred as storey).

The tubular metamaterials discussed above are subjected to two loading conditions: axial force and twisting moment (at the two ends, which is also occasionally referred as far-field actuation) in order to analyse the deformation mode coupling behaviour. A compressive axial force is applied in the vertical z-direction (i.e. longitudinal direction) on the top nodes, while the twisting moment is applied in the x-y plane (perpendicular to the tube axis) of the tubular metamaterial. These tubular metamaterials are modelled computationally according to the idealized bar-hinge approach (refer to Methods section

for a detailed discussion on the methodology) [75]. The discretization method used to analyse these tubular metamaterials is following a triangulated approach by N4B5 scheme. Besides computational modelling, we have created physical prototypes for qualitatively validating the mechanical constitutive behaviour, as depicted in supplementary videos SM1 - SM3. In the following discussions, the material properties used for the triangulated origami architecture I model is: folding stiffness (K_f) = 0.1 N/cm^2, bending stiffness (K_b) = 1×10^3 N/cm^2, stretching stiffness (E_o) = 1×10^6 N/cm^2, and idealized bar area (A_{bar}) = 0.1 cm^2. The material properties used for the triangulated origami architecture II and III model are: folding stiffness (K_f) = 1×10^{-3} N/cm^2, bending stiffness (K_b) = 1×10^{-3} N/cm^2, stretching stiffness (E_o) = 5×10^3 N/cm^2, and idealized bar area (A_{bar}) = 0.1 cm^2. Note that the bar-hinge based computational modelling approach adopted here is quantitatively validated for tubular origami architectures with separate experimental results (refer to supplementary material Figure S7 and supplementary note II) besides the qualitative validations presented in Figure 1 and supplementary videos SM1 - SM3, providing adequate confidence on the insights presented in this paper.

In the following subsections, we will first investigate qualitatively using physical prototypes as to how the origami crease architecture influences the deformation mode coupling behaviour. Subsequently, a detailed numerical investigation is presented to quantify the degree of axial-twist coupling and stability behaviour as a function of the crease architecture and motion stage.

2.1. Qualitative constitutive behaviour of tubular origami metamterials

When triangulated origami architecture I based tubes are subjected to a compressive force, they start compressing in the axial direction and also show outward or inward bulging due to deformation in lateral directions. This bulging changes with an increase in compressive force on the tube (refer to Figure 1(A)). The deformation behaviour of the triangulated origami architecture I based tube is qualitatively validated here with the deformation behaviour of a physical prototype under compression (refer to supplementary movie SM1). Negligible or no rotational deformation is shown under lower range of compressive axial forces. A more detailed analysis covering this aspect of shape morphing in triangulated origami architecture I based tubes as a function of crease architecture and motion stage can be found in literature [59].

When a similar triangulated origami architecture I based tube is subjected to a twisting moment, the creases of the tube initiate rotational deformation and aim to converge toward each other. This behaviour of creases results in the deformation of the tube in the axial direction. As the twisting moment on the structure increases, a corresponding increase in axial deformation is observed (refer to Figure 1(A)). The physical prototype under twisting further validates this deformation behaviour of the

triangulated origami architecture I based tube, as presented in the supplementary movie SM1.

When a triangulated origami architecture II based tube is subjected to compressive force, it shows axial deformation (and twisting deformation) due to the tube twisting. As the compressive force initiates its action, the central segment of the tube undergoes initial torsional deformation, consequently resulting in axial deformation. As the applied force increases, the structure transitions into multi-stable or mono-stable deformation depending on the crease architecture and dimensions, further increasing the level of axial deformation (refer to Figure 1(B)). The triangulated origami architecture II based tube deformation behaviour is validated with a physical prototype under compression (refer to supplementary movie SM2).

The triangulated origami architecture II based tube, under the application of a twisting moment, exhibits similar behaviour (i.e. both axial and twisting deformations) to that observed under compressive loading conditions. With the application of a twisting moment on a triangulated origami architecture II based tube, the last segment of the tube initially experiences torsional deformation and results in axial deformation. With the increase in the twisting moment, the structure enters into multiple stable states or follows a monostable path depending on crease dimensions, leading to increased axial contraction (refer to Figure 1(B)). A physical prototype under twisting validates this deformation behaviour of triangulated origami architecture II based tubes, as presented in supplementary movie SM2.

The triangulated origami architecture III based tube, under the action of compressive force, shows axial deformation-dominated behaviour. As the compressive force increases, the underlying kinematics of the tube allows axial deformation with very minimal rotation, resulting in a mostly decoupled axial and rotation motion (refer to Figure 1(C)). A physical prototype under compressive force validates this deformation behaviour of the triangulated origami architecture III based tube (refer to supplementary movie SM3).

When a similar triangulated origami architecture III based tube is under the application of a twisting moment, the tube undergoes minimal axial contraction. As the twisting moment increases, the tube exhibits predominant rotational motion resulting in minimal axial contraction (refer to Figure 1(C)). The triangulated origami architecture III based tube deformation behaviour is validated with a physical prototype under a twisting moment, as discussed in the supplementary movie SM3.

It is worth noting that both the triangulated origami architecture II and III based tubes can exhibit mono-stability, bi-stability and multi-stability depending on the geometric parameters and structural configuration, while the triangulated origami architecture I based tubes always show monostability. To be more specific, whether a triangulated origami architecture II or III based tube will undergo a series of bi-stable deformation (leading to multi-stability for a tube with multiple storeys) or mono-stable

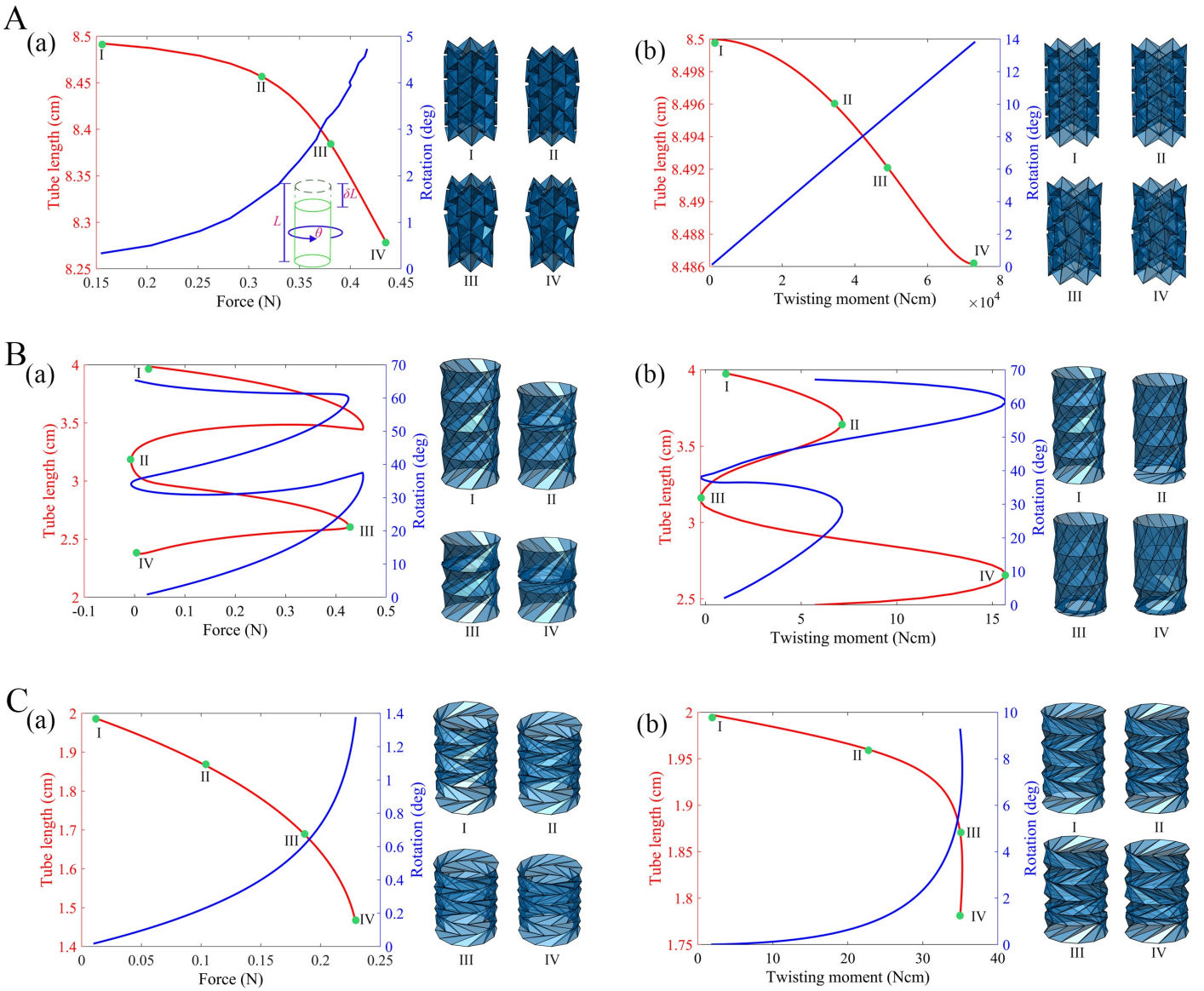

Figure 2: Numerical quantification of axial-twist mode coupling. Constitutive behaviour under the action of compressive force (F, in N), and twisting moment (M_t, in N-cm) for **(A)** Triangulated origami architecture I **(B)** Triangulated origami architecture II and **(C)** Triangulated origami architecture III. Subfigures (a) and (b) show results on mechanical deformation concerning axial and twisting modes under applied axial force and twisting moments respectively.

deformation, depends on the crease architecture. In case of multi-stability, it may be noted that the sequence of bi-stable deformation in both triangulated origami architecture II and III based tubes is highly dependent on the local imperfection and stiffness distribution in a physical sample, and it would be controlled by the rate of applying compressive force or torsional moment. The aspect of mono-stability and multi-stability is further numerically investigated in the following subsection based on mechanical constitutive behaviour. Under the application of compressive axial loading, all three tubes undergo some degree of axial deformation, but it is also compulsory for triangulated origami architecture II based tubes to undergo torsional deformation simultaneously. Triangulated origami architecture I and III based tubes can have predominantly axial deformation (without torsion, or with very little

value of it) under the application of compressive force. On the contrary, under the application of torsional moment, all three tubes undergo torsional deformation and they also show axial deformation simultaneously. It may be noted that the axial deformation of triangulated origami architecture III based tubes under the application of torsional moment is negligible compared to the other two architectures. This behaviour is primarily influenced by the middle crease of the triangulated origami architecture III unit, which induces a coupled axial-rotation motion that tries to maintain the total length of the tube constant. Furthermore, it can be concluded that the triangulated origami architecture III based tubes predominantly undergo decoupled axial and rotation motion on the free ends of the tube under axial compression and twisting moment.

To summarise the qualitative behaviour of the three different tubular architectures, we note the following salient points (refer to Figures 1, 2, S1, S2 and 4 along with corresponding supplementary videos SM1 to SM6).

Triangulated origami architecture I based tubular metamaterials: (1) Under axial force it shows only axial deformation (this is true up to a threshold limit of compressive force, beyond which there will be both twist and axial deformation - this aspect is discussed in detail later). Thus under low value of compressive force, no axial and twist coupling exists. (2) Under the application of twisting moments, there will be both twisting deformation and axial deformation simultaneously. Thus, there exists a axial-twist coupling under the application of twisting moment. (3) The triangulated origami architecture I based tubes always show a mono-stable behaviour. (4) There exists a significant lateral deformation under the application of axial and twisting forces, leading to a programmable spatially-varying bulging along the length of tubes [59].

Triangulated origami architecture II based tubular metamaterials: (1) Under axial force it shows both axial deformation and twisting simultaneously. (2) Under the application of twisting moments, there will be both twisting deformation and axial deformation simultaneously. Thus, there exists a axial-twist coupling under the application of both axial force and twisting moment. (3) The triangulated origami architecture II based tubes may exhibit mono-stable, bi-stable and multi-stable behaviour depending on the crease architecture. (4) The lateral deformation under the application of axial force or twisting moment is less significant compared to the triangulated origami architecture I based tubes.

Triangulated origami architecture III based tubular metamaterials: (1) Under axial force it shows predominantly axial deformation. (2) Under the application of twisting moments, there will be predominantly twisting deformation. Thus, there exists no (or less significant) axial-twist coupling under the application of both axial force and twisting moment. (3) The triangulated origami architecture

III based tubes may exhibit mono-stable, bi-stable and multi-stable behaviour depending on the crease architecture. (4) The lateral deformation under the application of axial force or twisting moment is less significant compared to the triangulated origami architecture I based tubes.

The primary nature of the current investigation is computational analysis, wherein the physical prototypes are used for qualitative validation of deformation modes as depicted in the supplementary videos (SM1-SM3). This qualitative analysis is intended to visually demonstrate the general characteristic constitutive behaviour identified for each of the triangulated origami architectures. Note that the bar-hinge-based reduced-order computational model is validated with quantitative experimental results concerning force-deformation (refer to Figure S7). This ensures that the computational predictions are accurate quantitatively. For a more detailed and rigorous assessment, we have performed comprehensive numerical analyses in the following subsection, which provide the quantitative data and predictions of the triangulated origami architectures. However, future experimental investigations are necessary to present quantitative experimental results and compare the current numerical findings in more detail.

The crease-dependent qualitative behaviour of tubular origami architectures, as discussed in this subsection, is substantiated quantitatively through a detailed numerical reduced order analysis in the following subsections.

2.2. Numerical quantification of the axial-twisting mode coupling

For each of the tubular structures having triangulated origami architecture I, II or III, compressive axial force and twisting moment will be applied separately in this subsection to study their axial deformation, twisting deformation and stability behaviour based on the bar-hinge based numerical model.

Under the initial stage of applying compressive force, the triangulated origami architecture I based tube shows a decrease in axial deformation as represented in configuration I (refer to Figure 2(A(a))). The geometry of the triangulated origami architecture I based tube is taken as: width = 2 cm, dihedral angle (α) = 55^o, and the number of bases longitudinally $m = 7$, and circumferentially $n = 6$. As the compressive force (F) starts increasing, the length of the triangulated origami architecture I based tube decreases more rapidly (as represented in configuration II) due to the folding of the creases. With further increment in the axial force (F), the axial deformation increases, along with outward bulging (as represented in configurations III and IV). Under the application of compressive force, slight twisting deformation is also observed along with axial deformation. The twisting of the triangulated origami architecture I based tube represented by rotation (θ) shows an increasing trend with the increase in axial compressive force. However, the value of twist throughout the considered range of applied axial force here is negligible. The increment in compressive force induces an increase in axial strain (ε) and a decrease in

the non-dimensional mode coupling factor (θ/ε) (refer to Figure S1(A(a))). The mode coupling factor, when compared with axial strain for a given applied force (or torsional moment, as discussed in the following paragraph), gives a sense of the relative twisting deformation with axial strain. It becomes evident that the twisting deformation here is negligible compared to axial deformation. The numerical results demonstrate negligible axial-twist coupling and mono-stability in the deformation behaviour of triangulated origami architecture I based tubes under the application of axial force. In this context, refer to the supplementary video SM1 showing the deformation behaviour obtained numerically and using physical prototypes. The behaviour of a triangulated origami architecture I based tube under compressive axial forces, as presented in this paragraph, is true up to a threshold limit of compressive force, beyond which there will be both twist and axial deformation - this aspect is discussed in detail later in the current section.

Further, we analyze a similar triangulated origami architecture I based tube under twisting moment (refer to Figure 2(A(b))). The geometry of the tube is taken as: width = 2 cm, dihedral angle (α) = 55^o, and the number of bases longitudinally $m = 7$, and circumferentially $n = 6$. The initial configuration of the triangulated origami architecture I based tube under zero twisting moment is represented by configuration I. An increase in the twisting moment (M_t), resulting in the twisting of the tube, leads also to an axial deformation of the triangulated origami architecture I based tube with respect to the initial configuration (represented by configurations II and III) (refer to Figure 2(A(b))). Configuration IV is achieved at a maximum axial deformation, maximal rotation (θ), and peak twisting moment (M_t) magnitude. The increase in twisting moment results in comparatively lower axial strain levels when compared to the strain experienced under compressive loading conditions. In addition, as the twisting moment increases, the mode coupling factor (θ/ε) curve demonstrates an asymptotic decline due to high values of rotational deformation (refer to Figure S1(A(b))). The numerical results demonstrate an axial-twist coupling and mono-stability in the deformation behaviour of triangulated origami architecture I based tubes under the application of twisting moment. In this context, refer to the supplementary video SM1 showing the deformation behaviour obtained numerically and using physical prototypes.

Now we shift our focus to the detailed numerical exploration of the deformation mode coupling behaviour of the triangulated origami architecture II based tube (refer to Figure 2(B(a))). The geometry of the triangulated origami architecture II based tube is taken as: height of each layer = 1 cm, angle (ϕ) = 45^o, and the number of bases longitudinally $m = 4$, and circumferentially $n = 12$. The initial configuration of the triangulated origami architecture II based tube under zero compressive loading (F) is represented by configuration I. With an increase in the compressive force (F), the central segment of

the tube initially starts folding by twisting, resulting in a decrease in the tube length. As the compressive force (F) reaches its peak value, it starts to decline and even enters the negative zone while the tube length decreases (represented by configuration II) along with an increase in rotation (θ). At this stage, the triangulated origami architecture II based tube undergoes substantial folding through twisting, leading to a bistable folding state. This state is characterized by a sudden decrease in tube length from configuration I and a sudden increase in rotation (refer to Figure 2(B(a))). After reaching the negative zone, the force value starts to increase and reaches another peak where the structure stabilizes into this state (represented by configuration III). After this peak, the force value again moves into the negative zone, but the tube length continues to decrease, while rotation increases, as the structure transitions toward another stable state, represented by configuration IV. As explained in Figure S1(B(a), during the initial increase in compressive force leading to the first peak, there is a rise in axial strain (ε) and the mode coupling factor (θ/ε). After reaching the peak force, as the force starts decreasing, the axial strain continues to increase, while the mode coupling factor decreases. With a further increase in the compressive force after entering the negative zone, the mode coupling factor begins to rise again. This behaviour of the mode coupling factor and axial strain highlights the bi-stable and multi-stable nature of the triangulated origami architecture II based tube with the considered crease architecture. Notably, the increase in axial strain and decrease in the mode coupling factor while achieving the first stable state is greater than that observed during the transition to the second stable state. From the comparative values of axial strain and mode coupling factor, it becomes evident that both axial strain and twisting rotation are significant during the deformation process for a given applied force value. In summary, the numerical results demonstrate a strong axial-twist coupling in the deformation behaviour of triangulated origami architecture II based tubes under the application of axial compressive force. In this context, refer to the supplementary video SM2 showing the deformation behaviour obtained numerically and using physical prototypes.

When the triangulated origami architecture II based tube is subjected to a twisting moment, the initial configuration of the tube under zero twisting moment (M_t) is demonstrated by configuration I (refer to Figure 2(B(b))). The geometry of the triangulated origami architecture II based tube is taken as: height of each layer = 1 cm, angle (ϕ) = 45^o, and the number of bases longitudinally $m = 4$, and circumferentially $n = 12$. With an increase in the twisting moment (M_t), the last segment of the triangulated origami architecture II based tube starts folding through twisting, resulting in a decrease of the tube length (represented by configuration II) and an increase in rotation (θ). After reaching at peak of a twisting moment, it starts decreasing and enters into a negative zone. At this stage, the

tube undergoes substantial folding through twisting, characterized by an abrupt decrease in tube length from configuration II to configuration III and a sudden increase in rotation (θ) attributed to a bi-stable folding state achieved by triangulated origami architecture II based tube (refer to Figure 2(B(b))). Following this negative phase, the twisting moment starts to increase again, reaching another peak that signals the transition to a new stable state, represented by configuration IV. The triangulated origami architecture II based tube with the considered crease dimensions, thus, exhibits multi-stable behaviour. The increment in the twisting moment (M_t) induces a sudden rise in axial strain (ε) and a corresponding decline in the mode coupling factor (θ/ε), which is attributed to the triangulated origami architecture II based tube's bi-stable and multi-stable nature (refer to Figure S1(B(b))). From the comparative values of axial strain and mode coupling factor, it becomes evident that both axial strain and twisting rotation are significant during the deformation process for a given applied twisting moment. In summary, the numerical results demonstrate a strong axial-twist coupling in the deformation behaviour of triangulated origami architecture II based tubes under the application of twisting moment. In this context, refer to the supplementary video SM2 showing the deformation behaviour obtained numerically and using physical prototypes.

Now, we focus on the deformation mode coupling behaviour of triangulated origami architecture III based tubes (refer to Figure 2(C(a))). The geometry of the tri-angulated origami architecture III based tube is taken as: height of each layer = 1 cm, angle (ϕ) = 45^o, and the number of bases longitudinally $m = 3$, and circumferentially $n = 12$. When the triangulated origami architecture III based tube is subjected to compressive force, with an increase in the compressive force (F), the tube shows compression in the axial direction (from configuration I to configuration IV) and a marginal increase in rotation (θ). The increment in compressive force (F) induces a rise in both strain (ε) and the mode coupling factor (θ/ε) (refer to Figure S1(C)). From the comparative values of axial strain and mode coupling factor, it becomes evident that both axial strain and twisting rotation are small during the deformation process for a given applied force, while the twisting rotation is negligible. In summary, the numerical results demonstrate a very weak (or negligible) axial-twist coupling in the deformation behaviour of triangulated origami architecture III based tubes under the application of axial compressive force. In this context, refer to the supplementary video SM3 showing the deformation behaviour obtained numerically and using physical prototypes.

Further, when the triangulated origami architecture III based tube is subjected to twisting moment (the geometry of the triangulated origami architecture III based tube is taken as: height of each layer = 1 cm, angle (ϕ) = 45^o, and the number of bases longitudinally $m = 3$, and circumferentially $n = 12$),

with an increase in the twisting moment (M_t), the tube initially starts folding through twisting, resulting in a decrease of the tube length (from configuration I to configuration IV) and an increase in rotation (θ) (refer to Figure 2(C(b))). The increment in the twisting moment (M_t) induces a rise in both axial strain (ε) and the mode coupling factor (θ/ε) (refer to Figure S1(C)). From the comparative values of axial strain and mode coupling factor, it becomes evident that both axial strain and twisting rotation are small during the deformation process for a given applied twisting moment, while the axial deformation is negligible. Further parametric study on the axial-twist mode coupling behaviour of triangulated origami architecture III is presented in Supplementary note I, which upholds similar trends. In summary, the numerical results demonstrate a very weak (or negligible) axial-twist coupling in the deformation behaviour of triangulated origami architecture III based tubes under the application of of twisting moment. In this context, refer to the supplementary video SM3 showing the deformation behaviour obtained numerically and using physical prototypes.

An important point to note from the above discussion is that triangulated origami architecture II based tube exhibits coupled axial-twist motion, while triangulated origami architecture III based tube exhibits decoupled (or very weakly coupled) axial-twist motion under the application of axial compressive force and twisting moment separately. In the numerical results presented in Figure 2, we demonstrate that triangulated origami architecture II based tubes show bi-stability and multi-stability, while triangulated origami architecture III based tubes show mono-stability. However, this is true for the considered crease architectures and geometry. It can be shown that both triangulated origami architecture II and III based tubes can exhibit mono-, bi- and multi-stability depending on the crease architecture (as discussed further later in this section), while it may be noted that triangulated origami architecture I based tubes are always mono-stable.

2.3. Energy landscape under far-field axial and twisting actuations

Different modes of deformations and their couplings are a manifestation of the energy landscape during the deformation process in triangulated origami architecture I, II or III based based tubes. To bring more insights, we investigate the total energy and different constituting energy components for the three crease patterns under consideration (refer to Figure 3). Note the total energy is defined as the summation of all energy contributions in the system, including the bar energy, bending energy and folding energy. The folding energy refers to the energy stored at the hinges due to rotational deformations. The geometry of the triangulated origami architecture I based tube is taken as: width = 2 cm, dihedral angle (α) = 55^o, and the number of bases longitudinally $m = 7$, and circumferentially $n = 6$. The geometry of the triangulated origami architecture II based tube is taken as: height of each layer

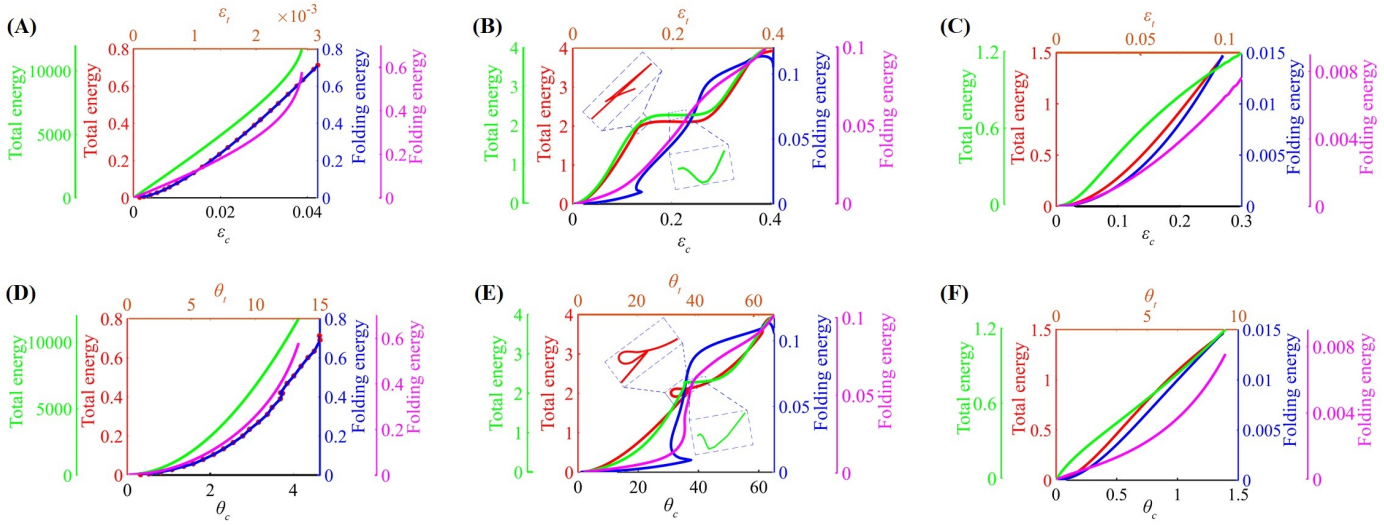

Figure 3: Energy landscape under axial and twisting modes. Energy landscape of tubular origami metamaterials under the action of far-field compressive force, and twisting moment. Total energy and folding energy are shown separately along with the corresponding axial strain and rotation under the application of axial force and twisting moment, respectively. **(A, D)** Triangulated origami architecture I **(B, E)** Triangulated origami architecture II **(C, F)** Triangulated origami architecture III. In each pair of subfigures ((A, D), (B, E) and (C, F)), the lower X axes of subfigures show the axial strain and corresponding twisting deformations, respectively under the application of axial force. The corresponding total energy and folding energy are presented using the red and blue-coloured Y axes, respectively. The upper X axes in each pair of subfigures show the axial strain and corresponding twisting deformations, respectively, under the application of twisting moment. The corresponding total energy and folding energy are presented using the green and purple-coloured Y axes, respectively. Note that the curves presented in the subplots follow same color coding as the respective Y axes.

= 1 cm, angle $(\phi) = 45^o$, and the number of bases longitudinally $m = 4$, and circumferentially $n = 12$. The geometry of the triangulated origami architecture III based tube is taken as: height of each layer = 1 cm, angle $(\phi) = 45^o$, and the number of bases longitudinally $m = 3$, and circumferentially $n = 12$. Each pair of subplots (triangulated origami architecture I - A, D; triangulated origami architecture II – B, E; triangulated origami architecture III – C, F) presents results for applied compressive load and twisting moment, showing the corresponding axial strain and twisting deformations. For example, in case of triangulated origami architecture I based tubes, the lower x-axes of subfigures A and D show the axial strain and corresponding twisting deformations, respectively under the application of axial force. The corresponding total energy and folding energy are presented using the red and blue-coloured Y axes, respectively. The upper x-axes of subfigures A and D show the axial strain and corresponding twisting deformations, respectively, under the application of twisting moment. The corresponding total energy and folding energy are presented using the green and purple-coloured Y axes, respectively. Note that the curves presented in the subplots follow same color coding as the respective Y axes. Similar color coding and legends are adopted for the other two pairs (B, E and C, F)) of subfigures in Figure 3.

For the triangulated origami architecture I based tube under compressive force, it can be observed that the total energy stored by the tube with axial strain (ε_c) and rotation (θ_c) primarily arises from the folding energy of creases, resulting in curve overlapping (refer to Figure 3(A)). In contrast, under the

application of the twisting moment, the total energy stored by the triangulated origami architecture I based tube concerning axial strain (ε_t) and rotation (θ_t) is mostly due to folding along creases, but the energy due to facet bending and deformation of the creases is higher compared to the case of applied axial force (refer to Figure 3(D)). In the case of triangulated origami architecture II based tubes, crease folding becomes significantly less predominant energy component and the contribution of facet bending and crease deformation energy shows one order higher magnitude (depending on the applied axial force or torsional moment) (refer to Figure 3(B, E)). The total energy plots show energy minima in this case for both cases of appplied external compression and twist (corresponding to the motion states of zero force and moments depicted in Figure 2(B)), indicating a bi-stable behaviour. The energy contribution of crease folding further reduces in the case of triangulated origami architecture III based tubes, and there cannot be spotted any energy optima related to the stability behaviour (refer to Figure 3(C, F)). The energy landscape concerning the proportions of folding energy and the remaining energy due to facet bending and deformation of the creases vary significantly for different origami architectures, leading to their distinct mechanical behaviour and stability characteristics.

As depicted in Figure 3(B, E)), the triangulated origami architecture II based tube experiences a snap-back instability, during which it undergoes a decrease in displacement at specific points to maintain the variation in force. The region, characterised by a simultaneous reduction in both displacement and force, is referred to as the snap-back instability region [76]. The simulation in this study is performed by employing the arc-length method [77], where equilibrium path of the force-displacement curve is determined by allowing both force and displacement to vary throughout each time step. Due to the nature of this approach, the applied load primarily indicates the direction of loading. The actual load applied in the first increment is obtained by multiplying the initial arc-length with the applied load. The behaviour of the force-displacement curve is influenced by the arc-length value, which can lead to either an instantaneous jump or snap-back instabilities [78]. The snap-back instability region generally forms to prevent the occurrence of an instantaneous jump. Within this region, a difference in total energy is observed, as shown in Figure 3(B). In general, the triangulated origami architecture II based tube always seeks to maintain a path with the lowest total energy. Within snap-back instability region, since the total energy of the next stable state is less, the triangulated origami architecture II based tube follows that path and achieves a bi-stable state without reverting to the snap-back path. Similar instability behaviour can be seen in Figure 3(E).

2.4. Remarks on stability states of triangulated origami architecture II and III based tubes under axial and twisting actuation

In the preceding discussions presented corresponding to Figure 2(B, C), the triangulated origami architecture II based tube shows bi-stability (and multi-stability), whereas the triangulated origami architecture III based tube shows mono-stability under compressive force and twisting moment for the given geometric parameters. However, when the geometry of the triangulated origami architecture II based tube is modified to a height of each layer = 0.41 cm, angle (ϕ) = 65^o, and triangulated origami architecture III based tube is set to a height of each layer = 1.75 cm and an angle (ϕ) = 60^o, while keeping the material properties unchanged, the stability behaviour reverses. With these crease architectures and geometry, the triangulated origami architecture II based tube exhibits mono-stability (refer to Figure S2(A)), whereas the triangulated origami architecture III based tube displays bi-stability (refer to Figure S2(B)), under the application of a compressive force or twisting moment. Thus, it can be concluded that the stability behaviour of the triangulated origami architecture II and III based tubes depends on the geometric parameters, and both of these configurations can show mono-, bi- and multi-stability.

In addition to the above remarks on stability behaviour, it can be noted that the axial-twist coupling behaviour of triangulated origami architecture II and III based tubes remains similar as discussed in the preceding paragraphs irrespective of the geometry (i.e. triangulated origami architecture II based tubes exhibit strong axial-twist coupling, while triangulated origami architecture III based tubes very less or negligible axial-twist coupling, as depicted in Figure S2). When a triangulated origami architecture III based tube with geometric parameters of layer height 1.75 cm and an angle (ϕ) = 60^o is subjected to the compressive force, a similar behaviour is observed, where the tube's length significantly decreases with a slight increase in rotation. When a triangulated origami architecture III based tube with geometric parameters of layer height 1.75 cm and an angle (ϕ) = 60^o is subjected to the twisting moment, the tube length decreases with significant increase in rotation. As the triangulated origami architecture III based tube transitions from configuration III to configuration IV, the decrease in tube length is evident, accompanied by a significant increased in rotation, as the middle crease of the last row of the tube attempts to rotate and maintain the tube's length (refer to Figure S2(B(a)). In general, the axial and rotational stiffness of the triangulated origami architecture III based tubes are much higher than that of the triangulated origami architecture I and II based tubes. In this context, refer to the supplementary videos SM4 and SM5 showing the deformation behaviour obtained numerically.

2.5. Parametric analysis of stability states in triangulated origami tubes under axial and twisting actuation

So far we have established that the triangulated origami architecture I is always monostable, while the triangulated origami architecture II and III can have both monostable and bistable (and multi-stable in case of multi-row configurations) behavior depending on the geometric parameters. We have presented atleast one configuration to support this statement. In this section, we have conducted a detailed parametric analysis to systematically investigate the trends of stability variation for the three triangulated origami architectures I, II and III. It will be apparent from the parametric variation of geometric and configurational attributes that an aspect of programmability in the motion-state-dependent stiffness exists in such tubular metamaterials, leading to the notion of "nonlinearity as functionality" in the constitutive behaviour for its prospective exploitation in niche engineering applications.

We first varied the number of circumferential units for all triangulated origami architectures while keeping the other parameters constant. For triangulated origami architecture I, the tube's geometry is defined as follows: width = 2 cm, dihedral angle (α) = 55^o, and the number of bases longitudinally $m = 7$. The circumferential units are varied as $n = 4$, 6, 8, respectively. It is noted that triangulated origami architecture I always exhibits monostability with the increase in the number of circumferential units n under both axial and twisting actuation (refer to Figure S3A(a,b) in the supplementary material).

For triangulated origami architecture II, the tube's geometry is defined as follows: height of each layer = 1 cm, angle (ϕ) = 45^o, and the number of bases longitudinally $m = 4$. The circumferential units are varied as $n = 8$, 12, 16, respectively. Interestingly, the triangulated origami architecture II exhibits bistability for the circumferential units $n = 8$ and = 12 under both axial and twisting actuation. However, the triangulated origami architecture II exhibits mono-stability when the number of circumferential units increases to 16 under both axial and twisting actuation. In this case, when the circumferential units are $n = 16$, the force (or moment) value decreases but doesn't achieve the negative force, which reflects the mono-stability behaviour. It can be concluded that as the number of circumferential units increases, the triangulated origami architecture II for this geometry loses bi-stability under both axial and twisting actuation (refer to Figure S3B(a,b) in the supplementary material).

For triangulated origami architecture III, the tube's geometry is defined as follows: height of each layer = 1 cm, angle (ϕ) = 45^o, and the number of bases longitudinally $m = 3$. The circumferential units are varied as $n = 8$, 12, 16, respectively. It is observed that the triangulated origami architecture III exhibits consistently mono-stability for all three considered cases under both axial and twisting actuation. In all these cases, force (or moment) doesn't achieve the negative value, which reflects the mono-stability behaviour in all three cases (refer to Figure S3C(a,b) in the supplementary material).

Having investigated the effect of the number of units in the circumferential direction, further parametric study is conducted by varying the geometric parameters (angle: α, ϕ) for triangulated origami architecture I, II and III in each of the units. For triangulated origami architecture I, the tube's geometry is defined as follows: width = 2 cm, the number of bases longitudinally $m = 7$, and circumferentially $n = 6$. The dihedral angle (α) is varied as 45^o, 50^o , 55^o, respectively. With the variation in the dihedral angle, the triangulated origami architecture I tube exhibits mono-stability under both axial and twisting actuation (refer to Figure S4A(a, b) in the supplementary material).

For triangulated origami architecture II, the tube's geometry is defined as follows: height of each layer = 1 cm, the number of bases longitudinally $m = 3$ and circumferentially $n = 12$. The angle (ϕ) is varied as 45^o, 50^o, 55^o, respectively. The triangulated origami architecture II exhibits bistability in all variations of the angle (ϕ). In all the cases, the tubes reflect a decrease in the force up to a negative value and then again increase under both axial and twisting actuation (refer to Figure S4B(a,b) in the supplementary material).

For triangulated origami architecture III, the tube's geometry is defined as follows: height of each layer = 1 cm, the number of bases longitudinally $m = 4$ and circumferentially $n = 12$ The angle (ϕ) is varied as 45^o, 50^o, 55^o, respectively. The triangulated origami architecture III exhibits mono-stability in all variations of the angle (ϕ) (refer to Figure S4C(a,b) in the supplementary material).

We have further explored the influence of the height of each layer (h) on the stability behaviour of triangulated origami architecture II and III. In this analysis, the triangulated origami architecture I is not considered since it has been firmly established here and in our earlier work [59] that these configurations are always monostable. For triangulated origami architecture II, the tube's geometry is defined as follows: angle (ϕ) = 65^o, the number of bases longitudinally $m = 4$ and circumferentially $n = 12$. The height of each layer h is varied as 0.5 cm, 0.8 cm, and 1 cm, respectively. Remarkably, when the layer height h is 0.5 cm, the triangulated origami architecture II shows mono-stability, while an increase in h to 0.8 cm and 1 cm shifts the behaviour to bi-stability. It can be concluded that the triangulated origami architecture II achieves bi-stability with an increase in the height of each layer h under both axial and twisting actuation (refer to Figure S5A(a,b) in the supplementary material).

For triangulated origami architecture III, the tube's geometry is defined as follows: angle (ϕ) = 60^o, the number of bases longitudinally $m = 3$ and circumferentially $n = 12$. The height of each layer h is varied as 0.5 cm, 0.875 cm, and 1 cm, respectively. It is observed that triangulated origami architecture III achieves bi-stability with an increase in the height of each layer h under both axial and twisting actuation (refer to Figure S5B(a,b) in the supplementary material). From the above discussion, it can

be concluded that hight (h) plays a crucial factor in achieving bi-stable behaviour and tailoring the energy barrier between stability states.

In general, the parametric study presented in this section, considering geometric and configurational attributes, upholds the earlier observations regarding the stability behaviour that triangulated origami architecture I is always monostable, while the triangulated origami architecture II and III can have both monostable and bistable (and multi-stable in case of multi-row configurations). However, such stability behaviour and the energy barriers (in triangulated origami architecture II and III) can be tailored significantly (and optimized under certain operational and manufacturing constraints) through such parametric variation.

2.6. Post-contraction twist in triangulated origami architecture I based tubes under axial force

In the preceding discussions concerning the deformation process of triangulated origami architecture I based tubes we have highlighted that a predominantly axial mode of deformation is exhibited under the application of axial loads. However, this is not valid for a very high amount of applied axial force and a post-contraction twisting deformation can be observed beyond a critical value of axial force. During this stage of deformation, the twist motion starts in the middle of the tube and successively spreads toward both ends [46]. Note that as a result of this twisting deformation, there exists axial deformation as well during the second phase of the deformation. In other words, the predominant deformation modes (and axial-twist mode coupling behaviour) of triangulated origami architecture I based tubes are dependent on the stage of deformation under the application of axial force. (1) There exists only predominant axial contraction in the first stage (covered in the preceding paragraphs) (2) Beyond a critical compressive load value, in the post-contraction second stage, there exists both axial and twisting deformations predominantly with a strong axial-twist mode coupling. In the following paragraphs, we demonstrate these two stages of deformation numerically based on the idealized bar and hinge based model for the first time.

The triangulated origami architecture I based tube is idealised as a reduced-order bar-hinge model with the geometric parameters as: width = 2 cm, dihedral angle (α) = 55^o, and the number of bases longitudinally $m = 7$, and circumferentially $n = 6$. The material properties used for the triangulated origami architecture I based tubular model is folding stiffness (K_f) = 0.1 N/cm^2, bending stiffness (K_b) = 1×10^3 N/cm^2, stretching stiffness (E_o) = 1×10^6 N/cm^2, and bar area (A_{bar}) = 0.1 cm^2. We have simulated the entire deformation process in the following stages: (1) During the first stage, only compressive load is applied as discussed in the preceding paragraphs. This stage only leads to compressive deformation until the maximum limit (corresponding to which the threshold compressive force is de-

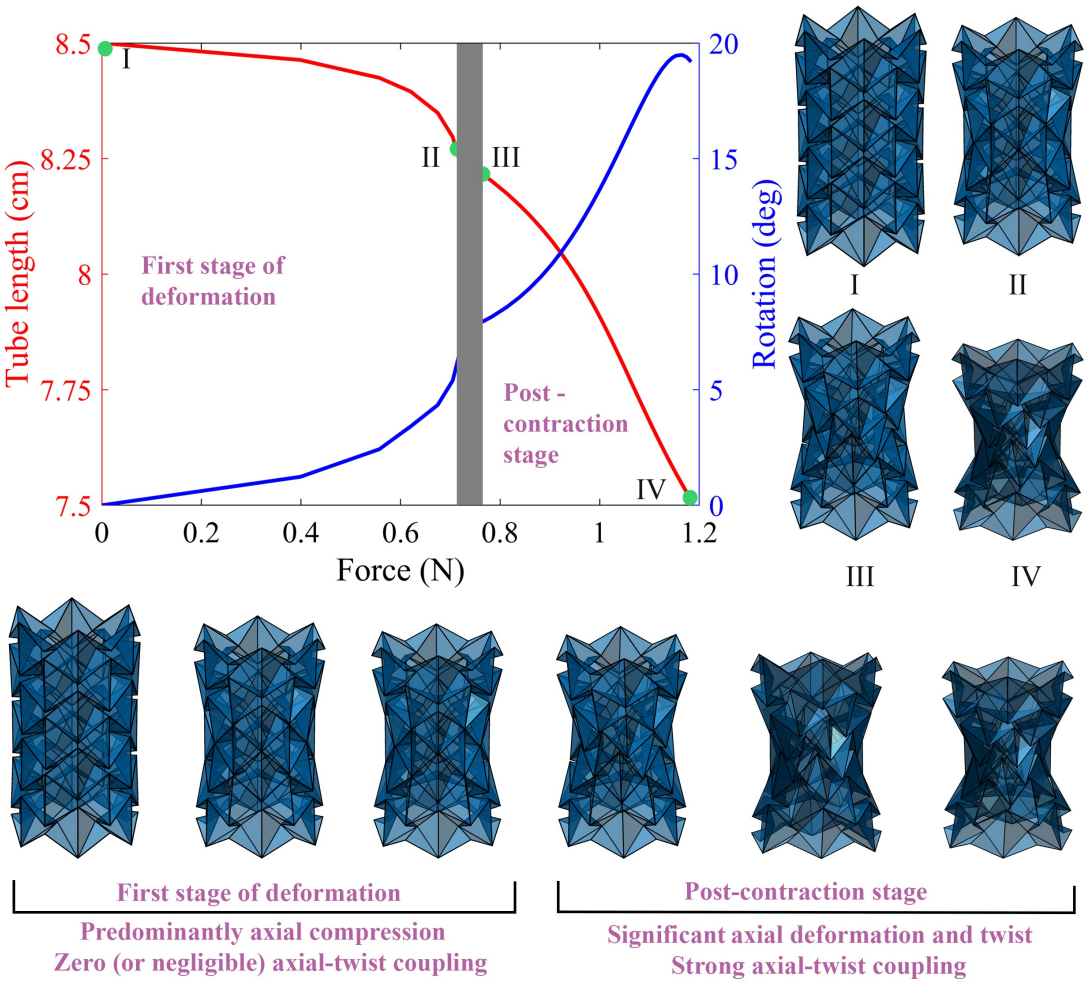

Figure 4: Post-contraction twist in triangulated origami architecture I under axial force. Simulated constitutive behaviour under the action of compressive force (F, in N) for triangulated origami architecture I. Both tube length and rotation (θ, in degree) are shown under axial force. It is shown that the predominant deformation modes (and axial-twist mode coupling behaviour) here are dependent on the stage of deformation under the application of axial force. (1) There exists only predominant axial contraction in the first stage. (2) Beyond a critical compressive load value, in the post-contraction second stage, there exists both axial and twisting deformations predominantly with a strong axial-twist mode coupling. Refer to Supplementary video SM6 for the entire simulation of different deformation stages.

fined) and no twisting deformation. (2) To initiate the twist, we adopt a very short intermediate stage (the starting origami configuration for which is the end point of stage 1), where the twisting mode is activated by applying a small value of twist at the middle row of the triangulated origami architecture I based tube. Note that this sort of approach is quite standard in finite element modeling of buckling/ instability to activate the instability mode. (3) In the third stage (the starting origami configuration for which is the end point of the short intermediate stage), referred to as post-contraction stage here, we remove the twisting moment and only apply compressive force, leading to both twisting and compressive deformations simultaneously.

During the first stage of contraction, as the compressive force increases, the length of the tube decreases with minimal rotation, resulting in predominant axial contraction (refer to Figure 4). In this

stage, the triangulated origami architecture I based tube transitions from configuration I to configuration II. Further, a slight twist is applied to the middle row of the tube's configuration II, resulting in configuration III. This configuration III then serves as the initial state for simulating the post-contraction stage. As further compression is applied (without any twisting moment), the twist motion starts from the middle rows and continues to spread in both directions, leading to a further reduction in tube length (refer to configuration IV). In this post-contraction stage, it is observed that the tube exhibits both rotational deformation and axial contraction. In this context, simulation of the entire deformation behaviour is presented in the supplementary video SM6.

2.7. Programmable Poynting and inverted Poynting effect

The deformation mode coupling behaviour of tubular origami metamaterials, as presented in the preceding paragraphs, shows a numerical quantification of the extent of coupling between axial and twisting deformations under applied axial force or twisting moment. This behaviour can be explained in terms of Poynting and inverted Poynting effect [79]. The Poynting effect is a non-linear elastic effect in which a cylinder expands axially under the application of torsion (or applied shear stress). A positive Poynting modulus causes shear-induced (or torsion-induced) normal expansion, while a negative Poynting modulus leads to normal contraction. When, on the contrary, an applied pure axial compression results in twisting (or shear) deformation, it is referred to as inverted Poynting effect. Generally, the Poynting effect adheres to the Maxwell-Betti reciprocity theorem, which demonstrates that identical shear displacements in the opposite directions result in equal normal stresses. However, in some lattice-based tubular metamaterials, this theorem is violated, leading to a phenomenon known as the non-reciprocal Poynting effect, where identical shear displacements in opposite directions induce unequal normal stresses [80]. In the current context, we deal with cylindrical tubes, where the Poynting and inverted Poynting effects are defined based on the coupling between axial and twisting modes.

From the numerical and physical insights on deformation mode coupling, as presented in the preceding section, we reveal that a programmable Poynting effect can be achieved in origami tubes as a function of crease architecture. If we only consider the predominant deformation modes of the three tubular origami architectures, the following inferences can be drawn. (1) Triangulated origami architecture I based tubes exhibit Poynting effect throughout the entire deformation under the application of twisting moment, but the inverse Poynting effect is only exhibited during the post-contraction deformation stage under the application of axial force. Thus, the exhibited inverse Poynting effect here is dependent on the motion stage. (2) Triangulated origami architecture II based tubes exhibit both Poynting effect and inverse Poynting effect throughout the deformation process. (3) The Poynting effect

and inverse Poynting effect are negligible in the case of triangulated origami architecture III based tubes.

2.8. Summary of contribution and contextualization

While the insightful works reporeted in literature (such as the mechanics of Kresling origami by Zang et al. [32]) provide an in-depth investigation of the coupling behaviour in Kresling origami with the same handedness, our study focuses on a broader objective, that is, the analysis of triangulated origami architectures for unravelling their constitutive coupling with a comparative perspective. In this context, the Kresling (with the same or opposite handedness) and waterbomb configurations are specific patterns that naturally fall within the class – generally referred to as tubular triangulated origami architectures. Please note the following points highlighting the contribution of the current work:

(1) In the existing literature, the intriguing aspect of deformation mode coupling between the axial and twisting modes in different classes of origami tubes has not been explored adequately. We present novel exploitable insights on tunable axial-twist coupling behaviour in tubular origami metamaterials, including the aspect of programming Poynting and inverse Poynting effects as a function of triangulated crease architecture. Rather than focusing on just a specific origami architecture (such as the Kresling origami, as investigated in literature [32]), we focus on exploring whether there can be twisting or axial deformation under the application of either axial or twisting far-field actuation in a compulsory or discretionary way, and the functional relationship to modulate such constitutive coupling through crease architecturing. Through rigorous numerical analyses and qualitative experiments, we establish the crease pattern-dependent characteristic features concerning such compulsory or discretionary coupling behaviour.

(2) The corresponding energy landscapes are investigated as an integral part, revealing their stability behaviour and the prospect of triangulated crease architecture-dependent tailoring of multi-stability, leading to establishing generic statements such as: triangulated origami architecture I is always monostable, while the triangulated origami architecture II and III can have both monostable and bistable (and multi-stable in case of multi-row configurations) behavior depending on the geometric parameters.

(3) Our study provides a numerical analysis of the post-contraction twisting behaviour of the triangulated origami pattern I, which has not been previously quantified through a bar-hinge based reduced order model, leading to novel insights concerning the Poynting and inverted Poynting effect under large axial deformations.

(4) *Supplementary notes on equivalent lattice architectures:* The primary focus of this paper is developing tubular origami based models consisting of creases and facets. However, in many cases, manufacturing

an engineering-grade origami architecture for achieving the necessary constitutive behavior may be challenging. Just to achieve the desired effective constitutive mechanical behavior as outlined in this paper, it is not always necessary to manufacture the exact origami tube with triangulated crease architecture. An idealized and equivalent lattice-based tube can be manufactured much easily, while retaining all the critical effective properties in terms of mode coupling and stability. For developing such a lattice tube, the construction should follow: (a) all the origami creases replaced by bar-like elements, (b) all the facets removed and (c) all the bars connected at the origami vertices where rotational springs should be implemented. Thus, the proposed results demonstrated using triangulated origami architectures are equally applicable to equivalent lattice tubes.

The coupling behavior between axial and twisting responses, including associated constitutive insights in terms of energy landscape, Poynting effect and unique large deformation behaviour has not been comprehensively studied before considering the generic class of triangulated origami architectures. In light of the above discussion, the novel and potentially impactful contribution reported in this manuscript will influence the design of a range of engineering systems for achieving bespoke mechanical behaviour demanding a high level of programmability in the constitutive behaviour.

3. Discussion

This article presents novel exploitable insights on deformation mode coupling behaviour of tubular origami metamaterials exploring whether there can be twisting or axial deformation under the application of axial or twisting far-field forces in a compulsory or discretionary way as a function of the crease architecture and motion state. Based on comprehensive computational and experimental investigations it is unravelled that the following constitutive behaviour can be achieved through crease architecturing as per application-specific demands: coupled axial and twisting modes under applied twisting moment (triangulated origami architecture I), motion state-dependent axial and twisting coupling behaviour under the application of axial force (triangulated origami architecture I, where decoupled constitutive behaviour is noticed with purely axial deformation under the application of lower values of axial force, but beyond a threshold value of axial force a coupled constitutive behaviour is demonstrated), coupled axial and twisting modes under the application of both axial force and twisting moments (triangulated origami architecture II), decoupled axial and twisting modes under the application of both axial force and twisting moments (triangulated origami architecture III). It is noted that the triangulated origami architecture I based tubes exhibit Poynting effect throughout the entire deformation process under the application of twisting moment, but the inverse Poynting effect is only exhibited during the

post-contraction deformation stage (i.e. beyond the threshold limit of axial force) under the application of axial force. Thus, the exhibited inverse Poynting effect here is dependent on the motion stage. Triangulated origami architecture II based tubes exhibit both Poynting effect and inverse Poynting effect throughout the deformation process, while both Poynting and inverse Poynting effects are negligible in the case of triangulated origami architecture III. The force-deformation constitutive behaviour and the energy landscape corresponding to different tubular origami metamaterials further reveal that it is possible to achieve mono-stability, bi-stability or multi-stability of different degree in triangulated origami architecture II and III through appropriate geometric design, while the triangulated origami architecture I invariably exhibit mono-stability. Notably, such constitutive programming in coupling behaviour, Poynting effect, energy landscape and stability behaviour is achievable through architecturing the creases based on a common triangulated pattern inscribed in the same intrinsic sheet of material.

In summary, we demonstrate that the exploitable nexus of crease architecture and folding mechanics can lead to programmable constitutive mode coupling and stability behaviour in tubular origami metamaterials, resulting in improved and unprecedented functionalities concerning efficient load distribution and conversion of deformation modes in wave propagation and steering, energy harvesting, vibration control, energy absorption, controlled deployment and mechanical computing.

Methods

Idealized computational modelling

The numerical analysis is carried out in this paper following a reduced order modelling approach of origami based on idealized bar-hinge model. The bar-hinge model is a simplified representation of the deformation mechanics of origami structures capturing the motion kinematics, where forces are considered to analyse the behaviour of origami structures. The origami structure with a bar framework undergoes basic forms of deformation: in-plane stretching and out-of-plane crease folding and bending. In the bar hinge model, the bars are placed along straight fold lines, whereas rotational hinges are placed along and across the bar connecting panels to model the crease folding and panels bending. The bar-hinge model reduces the degree of freedom of the overall model, resulting in efficient prediction of the mechanical behaviour of origami structures. The bar-hinge model is a mesh-dependent approach analysed with two triangular schemes, including N4B5 and N8B5 schemes. In the N4B5 scheme, the quadrilateral panel is divided into two panels by one of its diagonals. In contrast, in the N8B5 scheme, the quadrilateral panel is divided into four triangles by adding an extra internode. The number of triangles in the N8B5 scheme gives closer results to the physical model than the N4B5 scheme. The bar-hinge model can essentially be referred to as a reduced-order modeling approach since the important

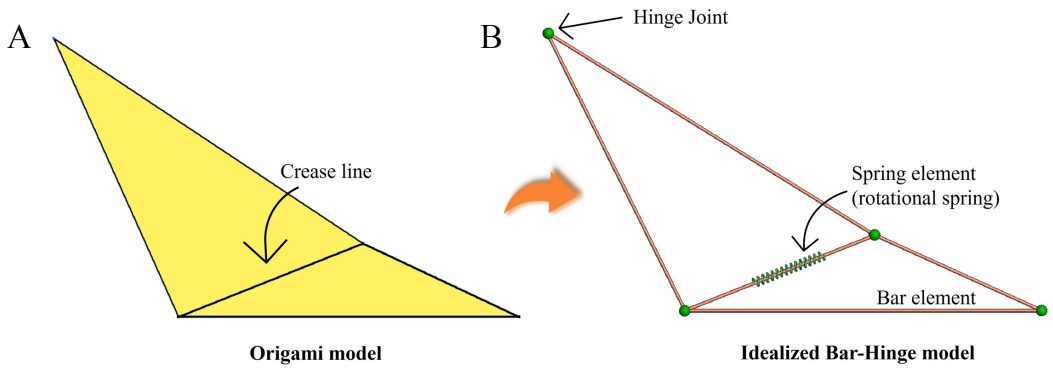

Figure 5: Bar-hinge model for idealising the structural behaviour of origami structure. Typical representation of **(A)** the actual folding model with two facets and one crease, **(B)** reduced order bar-hinge model.

features concerning load and deformation are captured accurately by adopting a simplified equivalent structural form of the origami. Origami codes such as MERLIN2 uses both N4B5 and N8B5 triangular scheme to analyse the origami structure [75, 77]. In the current work, the bar-hinge based idealized origami model is adopted considering the material and geometric attributes as described in the preceding sections for the three tubular origami architectures.

In the triangulated origami architectures, the triangular facet is modelled by bar elements, whereas the crease is considered equivalent to a rotational spring stiffness in this idealisation (refer to Figure 5). Assuming that the structure exhibits non-linear elasticity, we can express the total potential energy of this simplified origami model:

$$\Pi = U_{bar} + U_{spring} - V_{ext} \tag{1}$$

The potential energy contains three terms : U_{bar} denotes strain energy stored in bars, accounting for the in-plane deformation strain energy of the origami sheet, U_{spring} denotes strain energy stored in the bending and folding deformation accounting for the out-plane deformation strain energy and V_{ext} denotes the work done by external load. The equilibrium equation for an idealised bar-hinge-based model can be expressed as:

$$\frac{\partial U_{\text{bar}}}{\partial u} + \frac{\partial U_{\text{spring}}}{\partial u} = F \tag{2}$$

where u denotes the nodal displacement. Note that the stored energy in the system would depend upon the axial stiffness of bars EA, the rotational stiffness of springs along the fold lines K_f and bending stiffness of facets K_b [75, 77]. The above equation is solved following the modified generalised displacement control method, which is an arc-length type method leading to the whole equilibrium path of the displacement-controlled system [77].

In the current paper, we have followed the reduced order modelling approach, as described above, for obtaining all the computational results. However, from an analytical modelling perspective, the

far-field response of Type II and Type III tubes could also be analysed based on the behaviour of a single Kresling unit and its axial-twisting coupling. For a purely kinematic analysis, analysing a single Kresling unit can provide valuable insights into its mono-stability or bi-stability characteristics. However, since our study is based on numerical simulations that incorporate elasticity (stretching, bending, and folding deformation), accurately capturing the mechanical response of a single Kresling unit becomes challenging with difficulties in assigning appropriate Dirichlet and Neumann boundary conditions. In order to capture the response perfectly, an ideal boundary would need to be enforced, which is nontrivial in this reduced order simulation framework. Therefore, to obtain reliable numerical results, it is necessary to include a sufficient number of units along both the axial and circumferential directions for minimizing the boundary effects and ensure a meaningful and representative analysis of the overall structural behaviour.

Physical prototyping

Besides computational modelling, we have created physical prototypes for qualitatively validating the mechanical behaviour based on 300 GSM thick engineering-grade paper samples following the conventional process of creasing using Silhouette cutting machine, and subsequently folding and attaching the two opposite edges to form tubes. The qualitative constitutive behaviour of the physical prototypes is captured through motion recognition enabled high-quality cameras, as presented in Supplementary videos SM1 - SM3.

Data availability

All data sets used to generate the results are available in the main paper. Further details could be obtained from the corresponding authors upon reasonable request.

Acknowledgements

SN and TM would like to acknowledge the Initiation grant received from the University of Southampton during the period of this research work.

Author contributions

TM conceived the idea. AS prepared the results under the supervision of SN and TM. TM wrote the manuscript with contributions from SN.

Competing interests

I declare that the authors have no competing interests as defined by Nature Portfolio, or other interests that might be perceived to influence the results and/or discussion reported in this paper.

References

[1] P. Sinha, T. Mukhopadhyay, Programmable multi-physical mechanics of mechanical metamaterials, Materials Science and Engineering: R: Reports 155 (2023) 100745.

[2] X. Wu, Y. Su, J. Shi, Perspective of additive manufacturing for metamaterials development, Smart Materials and Structures 28 (9) (2019) 093001.

[3] M. Y. Khalid, Z. U. Arif, A. Tariq, M. Hossain, R. Umer, M. Bodaghi, 3d printing of active mechanical metamaterials: A critical review, Materials & Design (2024) 113305.

[4] T. Mukhopadhyay, S. Adhikari, A. Alu, Theoretical limits for negative elastic moduli in subacoustic lattice materials, Physical Review B 99 (9) (2019) 094108.

[5] T. Mukhopadhyay, S. Naskar, S. Adhikari, Anisotropy tailoring in geometrically isotropic multi-material lattices, Extreme Mechanics Letters 40 (2020) 100934.

[6] A. Singh, T. Mukhopadhyay, S. Adhikari, B. Bhattacharya, Active multi-physical modulation of poisson's ratios in composite piezoelectric lattices: on-demand sign reversal, Composite Structures 280 (2022) 114857.

[7] P. Prajwal, S. Ghuku, T. Mukhopadhyay, Large-deformation mechanics of anti-curvature lattice materials for mode-dependent enhancement of non-linear shear modulus, Mechanics of Materials 171 (2022) 104337.

[8] A. Sinha, T. Mukhopadhyay, Kirigami-inspired metamaterials for programming constitutive laws: Mixed-mode multidirectional auxeticity and contact-induced stiffness modulation, Iscience 25 (12) (2022).

[9] S. Mondal, T. Mukhopadhyay, S. Naskar, Active heterogeneous mode coupling in bi-level multi-physically architected metamaterials for temporal, on-demand and tunable programming, Communications Engineering 4 (1) (2025) 1–15.

[10] J. U. Surjadi, L. Gao, H. Du, X. Li, X. Xiong, N. X. Fang, Y. Lu, Mechanical metamaterials and their engineering applications, Advanced Engineering Materials 21 (3) (2019) 1800864.

[11] M. Kadic, G. W. Milton, M. van Hecke, M. Wegener, 3d metamaterials, Nature Reviews Physics 1 (3) (2019) 198–210.

[12] J. Fan, L. Zhang, S. Wei, Z. Zhang, S.-K. Choi, B. Song, Y. Shi, A review of additive manufacturing of metamaterials and developing trends, Materials Today 50 (2021) 303–328.

[13] T. Lim, A. Alderson, K. Alderson, Experimental studies on the impact properties of auxetic materials, Physica status solidi (b) 251 (2) (2014) 307–313.

[14] R. Hedayati, N. Roudbarian, S. Tahmasiyan, M. Bodaghi, Gradient origami metamaterials for

programming out-of-plane curvatures, Advanced Engineering Materials 25 (14) (2023) 2201838.

[15] O. Duncan, M. Chester, W. Wang, A. Alderson, T. Allen, Effect of twist on indentation resistance, Materials Today Communications 35 (2023) 105616.

[16] S. Janbaz, R. Hedayati, A. A. Zadpoor, Programming the shape-shifting of flat soft matter: from self-rolling/self-twisting materials to self-folding origami, Mater. Horiz. 3 (2016) 536–547.

[17] D. Misseroni, P. P. Pratapa, K. Liu, B. Kresling, Y. Chen, C. Daraio, G. H. Paulino, Origami engineering, Nature Reviews Methods Primers 4 (1) (2024) 40.

[18] A. A. Zadpoor, Mechanical meta-materials, Materials Horizons 3 (5) (2016) 371–381.

[19] Z. Zhai, L. Wu, H. Jiang, Mechanical metamaterials based on origami and kirigami, Applied Physics Reviews 8 (4) (2021).

[20] J. L. Silverberg, A. A. Evans, L. McLeod, R. C. Hayward, T. Hull, C. D. Santangelo, I. Cohen, Using origami design principles to fold reprogrammable mechanical metamaterials, science 345 (6197) (2014) 647–650.

[21] S. Liu, G. Lu, Y. Chen, Y. W. Leong, Deformation of the miura-ori patterned sheet, International Journal of Mechanical Sciences 99 (2015) 130–142.

[22] L. H. Dudte, E. Vouga, T. Tachi, L. Mahadevan, Programming curvature using origami tessellations, Nature materials 15 (5) (2016) 583–588.

[23] K. Bertoldi, V. Vitelli, J. Christensen, M. Van Hecke, Flexible mechanical metamaterials, Nature Reviews Materials 2 (11) (2017) 1–11.

[24] C. Lv, D. Krishnaraju, G. Konjevod, H. Yu, H. Jiang, Origami based mechanical metamaterials, Scientific reports 4 (1) (2014) 5979.

[25] Z. Zhai, Y. Wang, K. Lin, L. Wu, H. Jiang, In situ stiffness manipulation using elegant curved origami, Science advances 6 (47) (2020) eabe2000.

[26] Z. Zhai, Y. Wang, H. Jiang, Origami-inspired, on-demand deployable and collapsible mechanical metamaterials with tunable stiffness, Proceedings of the National Academy of Sciences 115 (9) (2018) 2032–2037.

[27] Z. Song, X. Wang, C. Lv, Y. An, M. Liang, T. Ma, D. He, Y.-J. Zheng, S.-Q. Huang, H. Yu, et al., Kirigami-based stretchable lithium-ion batteries, Scientific reports 5 (1) (2015) 10988.

[28] S. J. Callens, A. A. Zadpoor, From flat sheets to curved geometries: Origami and kirigami approaches, Materials Today 21 (3) (2018) 241–264.

[29] A. Sharma, S. Naskar, T. Mukhopadhyay, Multi-physically programmable tubular origami metamaterials: Exploitable nexus of geometry, folding mechanics and stimuli-responsive physics, In Press

(2025).

[30] Y. Miyazawa, H. Yasuda, H. Kim, J. H. Lynch, K. Tsujikawa, T. Kunimine, J. R. Raney, J. Yang, Heterogeneous origami-architected materials with variable stiffness, Communications Materials 2 (1) (2021) 110.

[31] S. Dong, Y. Yu, Numerical and experimental studies on capturing behaviors of the inflatable manipulator inspired by fluidic origami structures, Engineering Structures 245 (2021) 112840.

[32] S. Zang, D. Misseroni, T. Zhao, G. H. Paulino, Kresling origami mechanics explained: Experiments and theory, Journal of the Mechanics and Physics of Solids 188 (2024) 105630.

[33] H. Zhang, Mechanics analysis of functional origamis applicable in biomedical robots, IEEE/ASME Transactions on Mechatronics 27 (5) (2021) 2589–2599.

[34] H. Junfeng, W. Guilin, L. Jie, X. Liang, Y. M. Xie, A modular continuous robot constructed by miura-derived origami tubes, International Journal of Mechanical Sciences 261 (2024) 108690.

[35] M. von Rosen, Design of a bistable origami stent with pneumatic actuation, masters thesis, lulea university of technology (2023).

[36] S. Chen, J. Chen, X. Zhang, Z.-Y. Li, J. Li, Kirigami/origami: unfolding the new regime of advanced 3d microfabrication/nanofabrication with "folding", Light: Science & Applications 9 (1) (2020) 75.

[37] D. Melancon, B. Gorissen, C. J. García-Mora, C. Hoberman, K. Bertoldi, Multistable inflatable origami structures at the metre scale, Nature 592 (7855) (2021) 545–550.

[38] A. K. Brooks, S. Chakravarty, M. Ali, V. K. Yadavalli, Kirigami-inspired biodesign for applications in healthcare, Advanced Materials 34 (18) (2022) 2109550.

[39] D. Kim, T. Kim, Y.-G. Lee, 4d printed bifurcated stents with kirigami-inspired structures, JoVE (Journal of Visualized Experiments) (149) (2019) e59746.

[40] S. Babaee, Y. Shi, S. Abbasalizadeh, S. Tamang, K. Hess, J. E. Collins, K. Ishida, A. Lopes, M. Williams, M. Albaghdadi, et al., Kirigami-inspired stents for sustained local delivery of therapeutics, Nature Materials 20 (8) (2021) 1085–1092.

[41] A. Reid, F. Lechenault, S. Rica, M. Adda-Bedia, Geometry and design of origami bellows with tunable response, Physical Review E 95 (1) (2017) 013002.

[42] E. T. Filipov, G. H. Paulino, T. Tachi, Origami tubes with reconfigurable polygonal cross-sections, Proceedings of the Royal Society A: Mathematical, Physical and Engineering Sciences 472 (2185) (2016) 20150607.

[43] Y. Chen, H. Feng, J. Ma, R. Peng, Z. You, Symmetric waterbomb origami, Proceedings of the Royal Society A: Mathematical, Physical and Engineering Sciences 472 (2190) (2016) 20150846.

[44] J. Ma, H. Feng, Y. Chen, D. Hou, Z. You, Folding of tubular waterbomb, Research (2020).

[45] J. Ma, Z. You, Modelling of the waterbomb origami pattern and its applications, in: International Design Engineering Technical Conferences and Computers and Information in Engineering Conference, Vol. 46377, American Society of Mechanical Engineers, 2014, p. V05BT08A047.

[46] H. Feng, J. Ma, Y. Chen, Z. You, Twist of tubular mechanical metamaterials based on waterbomb origami, Scientific reports 8 (1) (2018) 9522.

[47] H. Jiang, W. Liu, H. Huang, Y. Wang, Parametric design of developable structure based on yoshimura origami pattern, Sustainable Structures (2022).

[48] J. Cai, X. Deng, Y. Xu, J. Feng, Motion analysis of a foldable barrel vault based on regular and irregular yoshimura origami, Journal of Mechanisms and Robotics 8 (2) (2016) 021017.

[49] J.-E. Suh, J.-H. Han, An origami-based adaptive vibration isolator with yoshimura-patterned reconfigurable module, Journal of Intelligent Material Systems and Structures 34 (18) (2023) 2157–2171.

[50] H. Sharma, O. Raj, S. Upadhyay, Boom packaging with yoshimura pattern: Geometrical and deformation analysis, in: Machines, Mechanism and Robotics: Proceedings of iNaCoMM 2019, Springer, 2022, pp. 955–964.

[51] Z. Zhang, W. Fan, Y. Long, J. Dai, J. Luo, S. Tang, Q. Lu, X. Wang, H. Wang, G. Chen, Hybrid-driven origami gripper with variable stiffness and finger length, Cyborg and Bionic Systems.

[52] K. Yang, S. Xu, J. Shen, S. Zhou, Y. M. Xie, Energy absorption of thin-walled tubes with pre-folded origami patterns: Numerical simulation and experimental verification, Thin-Walled Structures 103 (2016) 33–44.

[53] F. John, J. R. COOKE, Natural twist buckling in shells: from the hawkmoth's bellows to the deployable kresling-pattern and cylindrical miura-ori, in: Proceedings of the 6th International Conference on Computation of Shell and Spatial Structures IASS-IACM, 2008.

[54] C. Jianguo, D. Xiaowei, Z. Ya, F. Jian, T. Yongming, Bistable behavior of the cylindrical origami structure with kresling pattern, Journal of Mechanical Design 137 (6) (2015) 061406.

[55] J. Berre, F. Geiskopf, L. Rubbert, P. Renaud, Toward the design of kresling tower origami as a compliant building block, Journal of Mechanisms and Robotics 14 (4) (2022) 045002.

[56] S. M. Alipour, J. Arghavani, On the starting point in designing kresling origami, Aerospace Science and Technology 138 (2023) 108301.

[57] H. Sharma, A. Chaudhary, S. Upadhyay, Experimental verification of the bistable behavior of conical kresling origami, Thin-Walled Structures 190 (2023) 110980.

[58] A. Tiwari, S. Upadhyay, T. Mukhopadhyay, On introducing conicity in tubular origami metastruc-

tures for programming the nonlinear dynamics in an expanded design space, Journal of Sound and Vibration (2025) 118941.

[59] T. Mukhopadhyay, J. Ma, H. Feng, D. Hou, J. M. Gattas, Y. Chen, Z. You, Programmable stiffness and shape modulation in origami materials: Emergence of a distant actuation feature, Applied Materials Today 19 (2020) 100537.

[60] G. V. Rodrigues, M. A. Savi, Reduced-order model description of origami stent built with water-bomb pattern, International Journal of Applied Mechanics 13 (02) (2021) 2150016.

[61] L. Zhao, T. Zhang, Z. Shang, Design and implementation of origami robot ros-based slam and autonomous navigation, Plos one 19 (3) (2024) e0298951.

[62] L. M. Fonseca, G. V. Rodrigues, M. A. Savi, A. Paiva, Nonlinear dynamics of an origami wheel with shape memory alloy actuators, Chaos, Solitons & Fractals 122 (2019) 245–261.

[63] S. Li, J. J. Stampfli, H. J. Xu, E. Malkin, E. V. Diaz, D. Rus, R. J. Wood, A vacuum-driven origami "magic-ball" soft gripper, in: 2019 International Conference on Robotics and Automation (ICRA), IEEE, 2019, pp. 7401–7408.

[64] T. Zhao, X. Dang, K. Manos, S. Zang, J. Mandal, M. Chen, G. H. Paulino, Modular chiral origami metamaterials, Nature 640 (8060) (2025) 931–940.

[65] S. Wu, T. Zhao, Y. Zhu, G. H. Paulino, Modular multi-degree-of-freedom soft origami robots with reprogrammable electrothermal actuation, Proceedings of the National Academy of Sciences 121 (20) (2024) e2322625121.

[66] J. T. Bruton, Packing sheet materials into cylinders and prisms using origami-based approaches, Brigham Young University, 2016.

[67] M. Li, Z. Zhou, B. Hao, C. Yu, Y. Chen, J. Ma, Design and deformation analysis of an inflatable metallic cylinder based on the kresling origami pattern, Thin-Walled Structures 188 (2023) 110859.

[68] B. Kresling, The fifth fold: Complex symmetries in kresling-origami patterns, Symmetry: Culture and Science 31 (4) (2020) 403–416.

[69] C.-X. Liu, X. Wang, W. Liu, Y.-F. Yang, G.-L. Yu, Z. Liu, A physics-informed neural network for kresling origami structures, International Journal of Mechanical Sciences (2024) 109080.

[70] L. Huang, T. Xie, L. Yin, Magnetically-actuated intracorporeal biopsy robot based on kresling origami, Theoretical and Applied Mechanics Letters 15 (1) (2025) 100500.

[71] H. Yasuda, K. Yamaguchi, Y. Miyazawa, R. Wiebe, J. R. Raney, J. Yang, Data-driven prediction and analysis of chaotic origami dynamics, Communications Physics 3 (1) (2020) 168.

[72] J. Chung, M. Song, S.-H. Chung, W. Choi, S. Lee, Z.-H. Lin, J. Hong, S. Lee, Triangulated cylinder

origami-based piezoelectric/triboelectric hybrid generator to harvest coupled axial and rotational motion, Research (2021).

[73] L. S. Novelino, Q. Ze, S. Wu, G. H. Paulino, R. Zhao, Untethered control of functional origami microrobots with distributed actuation, Proceedings of the National Academy of Sciences 117 (39) (2020) 24096–24101.

[74] R. Masana, S. Khazaaleh, H. Alhussein, R. Crespo, M. Daqaq, An origami-inspired dynamically actuated binary switch, Applied Physics Letters 117 (8) (2020).

[75] K. Liu, G. Paulino, Highly efficient nonlinear structural analysis of origami assemblages using the merlin2 software, Origami 7 (2018) 1167–1182.

[76] A. Seyedkanani, A. Akbarzadeh, Magnetically assisted rotationally multistable metamaterials for tunable energy trapping–dissipation, Advanced Functional Materials 32 (52) (2022) 2207581.

[77] K. Liu, G. H. Paulino, Merlin: A matlab implementation to capture highly nonlinear behavior of non-rigid origami, in: Proceedings of IASS Annual Symposia, Vol. 2016, International Association for Shell and Spatial Structures (IASS), 2016, pp. 1–10.

[78] I. Leahu-Aluas, F. Abed-Meraim, A proposed set of popular limit-point buckling benchmark problems (2011).

[79] A. Ghorbani, D. Dykstra, C. Coulais, D. Bonn, E. van der Linden, M. Habibi, Inverted and programmable poynting effects in metamaterials, Advanced science 8 (20) (2021) 2102279.

[80] L. Dong, K. Zhou, D. Wang, Programmable nonreciprocal poynting effect enabled by lattice metamaterials, Science Advances 10 (24) (2024) eadl5774.